Quantitative interpretation of gold nanoparticle-based bioassays designed for detection of immunocomplex formation

Ye Zhou
Division of Solid State Physics, Lund University, SE-22100 Lund, Sweden and Division of Molecular Physics, Department of Physics, Chemistry and Biology, Linköping University, SE-58183 Linköping, Sweden

Hongxing Xu
Division of Solid State Physics, Lund University, SE-22100 Lund, Sweden and Institute of Physics, Chinese Academy of Science, Beijing 100080, China

Andreas B. Dahlin
Division of Solid State Physics, Lund University, SE-22100 Lund, Sweden

Jacob Vallkil, Carl A. K. Borrebaeck, and Christer Wingren
Department of Immunotechnology, Lund University, SE-22007 Lund, Sweden

Bo Liedberg
Division of Molecular Physics, Department of Physics, Chemistry and Biology, Linköping University, SE-58183 Linköping, Sweden

Fredrik Höök[a)]
Division of Solid State Physics, Lund University, SE-22100 Lund, Sweden

(Received 8 December 2006; accepted 22 January 2007; published 29 March 2007)

The authors present in this paper how the extended Mie theory can be used to translate not only end-point data but also *temporal variations* of extinction peak-position changes, $\Delta\lambda_{peak}(t)$, into absolute mass uptake, $\Gamma(t)$, upon biomacromolecule binding to localized surface plasmon resonance (SPR) active nanoparticles (NPs). The theoretical analysis is applied on a novel sensor template composed of a three-layer surface architecture based on (i) a self-assembled monolayer of $HS(CH_2)_{15}COOH$, (ii) a 1:1 mixture of biotinylated and pure poly(L-lysine)-graft-poly(ethylene glycol) (PLL-g-PEG), and (iii) NeutrAvidin. Assisted by independent estimations of the thickness of the three-layer architecture using quartz crystal microbalance with dissipation (QCM-D) monitoring, excellent agreement with parallel mass-uptake estimations using planar SPR is obtained. Furthermore, unspecific binding of serum to PLL-g-PEG was shown to be below the detection limit, making the surface architecture ideally suited for label-free detection of immunoreactions. To ensure that the immunocomplex formation occurred within the limited sensing depth ($\sim$10 nm) of the NPs, a compact model system composed of a biotinylated human recombinant single-chain antibody fragment ($\varnothing \sim 2$ nm) directed against cholera toxin was selected. By tracking changes in the centroid (center of mass) of the extinction peak, rather than the actual peak position, signal-to-noise levels and long-term stability upon cholera toxin detection are demonstrated to be competitive with results obtained using conventional SPR and state-of-the-art QCM-D data. © *2007 American Vacuum Society.* [DOI: 10.1116/1.2700235]

I. INTRODUCTION

In the life sciences there is currently an eager search for methods that enable simple but efficient and sensitive affinity-based detection schemes for the analysis of biomolecular interactions.[1] Preferred designs should not require labeling of the target analyte with, e.g., fluorescent dyes or radioactive markers, as such labels may interfere with the biorecognition reactions under investigation. In addition, the labeling process introduces an additional time-consuming step in the analysis, and it is generally difficult to homogeneously label multiple targets in an unknown, complex biological sample. Bearing in mind present efforts to realize integrated laboratory-on-a-chip and array-based systems, the localized surface plasmon resonance (LSPR) phenomenon, which is achieved when light couples to collective oscillations in the surface electron plasma of noble metal nanoscale features, appears as especially attractive.[2,3] The reasons for this are manifold. First, in analogy with conventional SPR, a change in interfacial refractive index (RI) upon biomolecule binding induces a change in the position of the absorption band (color) of LSPR-active sensor substrates, thus providing an easily detectable optical signal using conventional transmission-absorption spectroscopy, as first demonstrated by Englebienne in studies of antibody-antigen interactions.[4] Second, the confinement of the LSPR phenomena to nanometric structures allows for extreme miniaturization down to the scale of single nanoparticles, which was first demonstrated in biological sensor applications using dark field microscopy of individual silver nanoparticles (NPs).[5,6] Third,

[a)]Author to whom correspondence should be addressed; electronic mail: fredrik.hook@ftf.lth.se.

both the sensitivity and sensing depth can be varied by varying the type of metal,[7,8] size,[9,10] shape,[10,11] and/or arrangement[12,13] of the nanostructures, thus enabling precise fine-tuning of the sensor template to the dimensions of the actual biological system under investigation. This makes the LSPR concept in several respects more attractive than conventional planar SPR, in which the laterally propagating nature of the surface plasmon polaritons puts strong demands on the optical alignment required for proper excitation and readout[14] and limits the lateral resolution to approximately 5 μm (Ref. 15) or even more in the near-IR regime, in which the sensitivity is highest.[16] Furthermore, in comparison with typical LSPR substrates, the penetration depth of the evanescent field associated with planar SPR is approximately one order of magnitude larger.[14] Hence, changes in bulk properties often interfere with and complicate the analysis of interfacial binding reactions. An advantage of planar SPR over LSPR is, however, the existence of sufficient theoretical descriptions and even analytical expressions that are capable of translating the measured response into absolute mass uptake.[17,18] In contrast, efforts on translating the observed peak-position or extinction-magnitude changes of LSPR-active NPs into absolute mass uptake is limited, and there are only a few reports on semiquantitative estimations[19,20] and quantification of bound amount in terms of layer thickness at saturated binding.[21,22] Although binding constants can still be determined by recording the rates of binding/unbinding alone, or in simple cases, by monitoring the saturated response versus concentration,[22–24] a measure of the absolute mass uptake is a prerequisite in many other situations. For instance, estimations of reaction kinetics in terms of mass transport require a precise determination of variations in the bound mass,[25] as does an accurate determination of the stoichiometric relation between different types of interacting entities.

To represent the extinction peak of LSPR NPs and changes in the same induced by changes in the interfacial RI upon biomacromolecule binding, the extended Mie theory was previously proven sufficient for spherical NPs, in which case interfacial binding was represented by films with homogeneous thicknesses d_{film} and refractive indices n_{film}.[26,27] It was also shown by Van Duyne and co-workers that more advanced theoretical models could represent the color changes of, for example, triangular shaped Ag particles.[28,29] By knowing both d_{film} and n_{film}, which may be obtained from such modeling, it is possible to estimate the mass uptake Γ using the formalism introduced by De Feijter *et al.*:[30]

$$\Gamma_i = d_{i,\mathrm{film}} \frac{(n_{i,\mathrm{film}} - n_m)}{(\partial n/\partial C)_i} = \frac{d_{i,\mathrm{film}} \Delta n_{i,\mathrm{film}}}{(\partial n/\partial C)_i}, \quad (1)$$

where n_m is the refractive index of the medium and $\partial n/\partial C$ the bulk-refractive index increment for the analyzed molecules. (The subscript i refers to subsequently formed layers as described below.) However, to theoretically represent peak-position changes of LSPR-active substrates upon thin-film formation, either d_{film} or Δn_{film} must be known (or assumed), followed by a fitting procedure, giving the value of n_{film} (or Δd_{film}) that best represents the experimentally observed change in peak position, $\Delta\lambda_{\mathrm{peak}}$.[22,27,31] This holds true also for conventional SPR, but for sufficiently thin films (defined as approximately one-tenth of the penetration depth),[17,18] it was shown that irrespective of the value chosen for d_{film} (or Δn_{film}), the product between Δd_{film} and Δn_{film} remains constant.[17] In the framework of Eq. (1), this means that the coupled mass ($\propto d_{\mathrm{film}} \Delta n_{\mathrm{film}}$) remains constant and can be trusted with high accuracy—even if neither the film thickness nor the film refractive index is known in advance. In contrast, since the evanescent field associated with LSPR sensors is on the order of one magnitude more shallow than that associated with planar SPR,[9,26,32,33] this rule is less likely to be applicable for LSPR sensors.

With the aim of arriving at a generic semianalytical expression for the translation of temporal variations in the peak position, $\Delta\lambda_{\mathrm{peak}}(t)$, into absolute mass uptake, $\Gamma(t)$, of LSPR-active NP sensors, we present a thorough analysis of the sensitivity of Eq. (1) to the initial choice of d_{film} (or Δn_{film}) using a refined variant of the extended Mie theory[26] (as described in the Supplementary Information,[57] the theory takes into account not only the underlying substrate but also particle-particle coupling).

The sensing template utilized engages a self-assembled monolayer (SAM) of COOH-terminated thiols, which is shown to enable efficient binding of biotin-modified poly(L-lysine)-graft-poly(ethylene glycol) (PLL-g-PEG) (PLL-g-PEGbiotin) and which was previously shown to be superior over, for example, traditional PEG-modified thiols with respect to suppressed unspecific protein adsorption from complex suspensions such as serum.[34,35] PLL-g-PEGbiotin provides also an attractive template for subsequent coupling of NeutrAvidin (or its analog streptavidin or avidin) and subsequent coupling of biotinylated compounds.[36] Simultaneously, this three-layer architecture (SH-COOH, PLL-g-PEGbiotin, NeutrAvidin) provides a good model system to evaluate the mass uptake obtained using the Mie-based theoretical modeling. This is because the utilized COOH-terminated SAM was previously characterized in great detail, revealing a film thickness of $\sim$2.2 nm with a packing density of 21.4 Å^2 per molecule on planar (111) Au surfaces.[37] In addition, the mass uptake of PLL-g-PEG on negatively charged planar surfaces, including COOH-modified Au, was previously characterized using both conventional SPR and optical waveguide laser spectroscopy, as was the subsequent binding of streptavidin (and its analog NeutrAvidin).[38]

It is also shown in this work that changes in the peak position, $\Delta\lambda_{\mathrm{peak}}$, of LSPR-active gold NPs can, in analogy with conventional SPR (Ref. 39) and LSPR-active nanoscale holes in planar gold films,[40] be recorded by tracking the centroid (center of mass) of the extinction peak with a resolution of better than $\sim 10^{-3}$ nm at a temporal resolution of <2 s. When combined with the generic algorithm developed to translate $\Delta\lambda_{\mathrm{peak}}$ ($\propto \Delta\lambda_{\mathrm{centroid}}$) into mass uptake Γ, it is shown how variations in mass uptake can be followed in real time for all steps in the three-layer architecture. This analysis thus provides an improved basis for a comparison between LSPR

sensors and alternative sensor designs in terms of absolute sensitivity and absolute mass uptake as illustrated using conventional planar SPR, which is physically similar in nature to LSPR, and quartz crystal microbalance with dissipation (QCM-D) measurements. Furthermore, besides information about coupled mass, an independent means of determining the film thickness is obtained from the QCM-D data.[41] In order to arrive at the correct mass uptake for films with a thickness of ~5 nm and above, this type of independent estimate of the film thickness is shown to be important. Finally, since the total film thickness after NeutrAvidin binding to PLL-g-PEG is as high as ~15 nm, subsequent coupling of biotinylated compounds will occur in a region where the sensitivity is significantly reduced. To use this LSPR sensor design to record, for example, immunoreactions, there is thus a need for alternatives to the typically utilized, and in this context, bulky IgG antibodies. This was achieved by the use of biotinylated single-chain antibody fragment (with a diameter as small as ~2 nm).[42] In this way, efficient detection of cholera toxin using the LSPR platform is demonstrated and proven competitive in signal-to-noise level and long-term stability with both conventional SPR and QCM-D.

II. EXPERIMENT

A. Materials

Gold chloride hydrate ($HAuCl_4 \cdot 3H_2O$) and sodium citrate tribasic dehydrate were purchased from Sigma-Aldrich. 3-aminopropyltriethoxysilane (APTES, 99%) was purchased from Sigma-Aldrich. 16-mercaptohexadecanoic acid (SAM-COOH) was obtained from Prof. Allara, Pennsylvania State University. PLL-g-PEG [molecular weight (MW) ~68 kDa], PLL-g-PEGbiotin (MW ~87 kDa), and NeutrAvidin (MW ~60 kDa) were purchased from Surface Solutions (Switzerland), human recombinant single-chain Fv (scFv) antibody (clone CT17, MW ~28 kDa) specific for cholera toxin subunit B (CT, MW ~11.6 kDa, Sigma-Aldrich) was selected from the n-CoDeR library,[43] and kindly provided by Bioinvent Int., Lund, Sweden. CT17 was produced in E. coli and purified by affinity chromatography on a Ni^{2+}-NTA gel (Qiagen, Hilden, Germany), dialyzed against PBS and stored at 4 °C until use. Purified CT-17 was biotinylated at a molar ratio of 1:5 (scFv:biotin) using EZ-Link Sulfo-NHS-LC-biotin (Pierce, Rockford, IL) as described by the manufacturer. Biotinylated scFv (biotin-CT17) was extensively dialyzed against PBS and stored at 4 °C until use. The specificity and functionality of the scFv have been thoroughly examined during both the selection procedure and in conventional antibody microarrays.[44]

B. Methods

The gold NPs and the NP-modified substrates were analyzed with transmission electron microscopy (TEM, Philips CM20 Ultra-Twin lens high-resolution microscope) and atomic force microscopy (AFM, Vecco Dimension 3100). The three-layer surface architecture (see below) was characterized with QCM-D monitoring (D300, Q-Sense AB, Sweden), described in detail elsewhere,[45,46] and surface plasmon resonance (Biacore 2000, Biacore Int., Sweden) in batch and flow (5 μl/min) modes, respectively. The planar substrates were gold-coated polished 5 MHz AT-cut crystals (Q-Sense AB) and gold-coated SPR chips (Biacore Int.). Transmission mode extinction spectra of the LSPR-active substrates were collected using a homebuilt design described in detail elsewhere,[47] including a 20 W tungsten-halogen white light source (Ocean Optics), a photo diode array detector (B&WTek, USA), and a software designed to record changes in both absolute peak position, $\Delta\lambda_{peak}$, and the centroid of the peak, $\Delta\lambda_{centroid}$.[47] A homebuilt flow cell with a measurement volume of ~500 μl was used for the LSPR measurements, which were recorded under stagnant conditions after a rapid (<1 s) exchange of the total liquid volume.

C. Surface preparations

Suspensions of colloidal gold were prepared using sodium citrate reduction of $HAuCl_4 \cdot 3H_2O$, as described elsewhere.[9] In brief, 400 μl $HAuCl_4 \cdot 3H_2O$ solution and 400 μl sodium citrate solution were simultaneously added to 75 ml vigorously boiling water. The liquid was stirred and the flask was connected to a reflux condensation system. During the reduction reaction, the color of the suspension changed from pale yellow via intense purple to ruby-red, after which it was cooled to room temperature under continuous stirring. The particle diameter was controlled by the ratio between $HAuCl_4 \cdot 3H_2O$ and sodium citrate to yield gold NPs with a diameter of ~40 nm.[9] This was consistent with the TEM analysis [inset in Fig. 1(a)], revealing slightly elliptically shaped NPs (major axis: 42.1±5.5 nm; minor axis: 33.9±3.7 nm). Glass substrates (Deckgläser, Germany, 25 mm diameter) were cleaned in piranha solution (3:1 mixture of concentrated H_2SO_4 and 25% H_2O_2) (note that care should be taken since piranha solution is very energetic and potentially explosive) for 30 min, followed by thorough rinsing in MilliQ water and drying with N_2. The substrates were then immersed in a 5:1:1 mixture of MilliQ water, 25% hydrogen peroxide, and 30% ammonia for 15 min at 80 °C, followed by thorough rinsing with MilliQ water and drying with N_2. The cleaned substrates were immediately enclosed in a low vacuum chamber at 60 °C, followed by addition of 200 μl APTES silane to a small holder next to the glass substrates for 10 min. The temperature was then increased to 150 °C for 1 h, enabling efficient gas-phase deposition and cross-linking of APTES. The substrates were finally rinsed in xylene and sonicated for 2 min. After drying in N_2, the substrates were incubated in the gold NP suspension for 24 h at 25 °C. Figure 1(a) shows an AFM image of Au NPs deposited on glass. An evaluation of the height histogram yielded a typical distribution in diameter of 35.1±5.5 nm, which is consistent with the TEM image. A fit of extinction spectrum to the extended Mie theory yields an average diameter of 36 nm (see legend to Fig. 1), which is in good agreement with the AFM and TEM analyses.

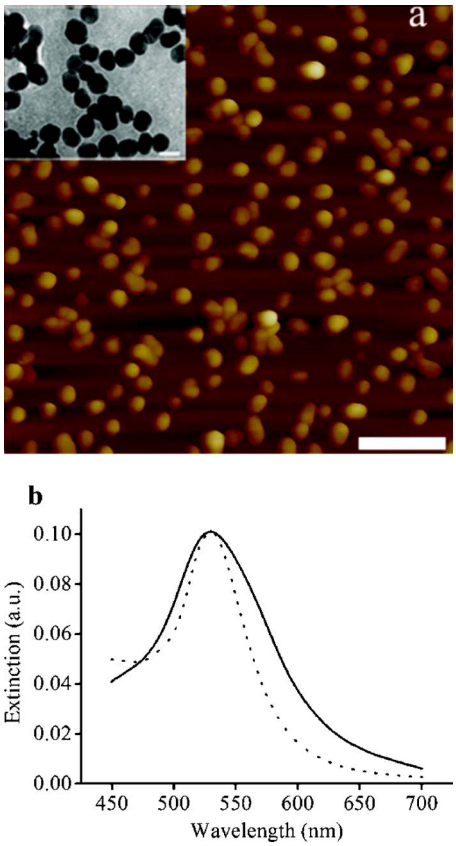

FIG. 1. Characterization of the Au NPs. (a) AFM image of a gold nanoparticle-coated glass, ~0.4 μm, the inset figure displaying a TEM image, ~40 nm. (b) Extinction spectrum of Au NPs deposited on glass (solid line) and theoretical simulation (dash line). The radius of the NPs is defined as a Gaussian distribution with a center radius of 18 nm and a standard deviation of 5.5 nm. The theoretical extinction spectrum also includes the effects of the substrate ($n=1.6$) and an interparticle coupling using a center-to-center distance of 125 nm and a particle density of 61/μm^2.

D. Measurement protocols

To avoid possible influence of binding of biotin moieties to the gold substrate and to provide a negatively charged surface, the gold substrates were modified with a spacer layer of $HS(CH_2)_{15}COOH$ (SH-COOH) prior to addition of PLL-g-PEGbiotin–PLL-g-PEG mixtures. For the planar gold substrates (SPR gold chips, obtained as gifts from Biacore Int., Sweden, and gold-coated QCM crystals from (Q-Sense AB, Sweden), this was done by incubation in a 1 mM SAM-COOH suspension (99.5% ethanol as solvent, Kmetyl, Sweden) for 24 h. After sonication and thorough rinsing in water, the chips were mounded in the SPR and QCM-D measurement chambers, respectively, followed by addition of a mixture of a 1:1 molar mixture of PLL-g-PEG and PLL-g-PEGbiotin at a total concentration of 100 μg/ml in HEPES1 buffer [4-(2-hydroxyethyl)piperazine-1-ethane-sulfonic acid, 10 mM HEPES, *p*H 7.4]. After saturated binding of PLL-g-PEGbiotin–PLL-g-PEG, NeutrAvidin (50 μg/ml) in HEPES2 buffer (10 mM HEPES, 150 mM NaCl, *p*H 7.4) was added followed by addition of biotin-CT17 (1.5 μg/ml in HEPES2 buffer) and cholera toxin (10 μg/ml in HEPES2 buffer). The same conditions were used for the gold NP-modified substrates, with the exception that the binding of SH-COOH was recorded in real time (see below). The 1:1 ratio of PLL-g-PEG and PLL-g-PEGbiotin was proven to provide an optimal binding capacity for subsequent binding of NeutrAvidin and biotinylated compounds (not shown), and the introduction of the SAM of SH-COOH as an adhesion layer for the PLL-g-PEG mixture was shown to reduce nonspecific binding from serum to $<2\%$ of that obtained on bare gold and $<20\%$ of that obtained on PLL-g-PEG-modified nonthiolated gold substrates (not shown).

III. RESULTS AND DISCUSSION

A. Estimation of the absolute mass uptake

The refined variant of the extended Mie theory (Supplementary Information[57]) was used to characterize the spectral variations of immobilized NPs upon formation of a SAM of HS-COOH in ethanol [Fig. 2(a)], followed by subsequent additions of PLL-g-PEG–PLL-g-PEG-biotin (1:1) and NeutrAvidin [Fig. 2(b)].

The theoretical representation of the spectral change in Fig. 2(a) was obtained by first assuming a thickness of 2.2 nm of the SAM film,[37,48] which was also confirmed by in house ellipsometric measurements on planar gold revealing a thickness of 22.2±0.7 Å on planar gold surface. This was followed by a fitting procedure in which the film refractive index was varied until a spectrum that matched the experimentally observed peak-position change was obtained. A perfect match to the peak position could be obtained by scarifying a match to the extinction magnitude, and vice versa. However, in terms of estimating the mass uptake based on this fit, the slight deviation observed in Fig. 2(b) has insignificant influence (see further below). The parameters (d_{film} and n_{film}) representing the SAM were then kept constant (see figure legend) when the core-shell model was used to represent the spectral changes observed on subsequently formed films [Fig. 2(b)]. It turned out from this fitting procedure that *independent* of the choice of film thickness, it was possible to find a film refractive index value capable of representing both the observed peak-position change and extinction increase equally well. Hence, the theoretical representation *cannot* be used to independently determine both the film thickness and the film refractive index. This is in direct analogy with previous SPR data.[17] However, in the case of conventional SPR, it was observed that the product between d_{film} and Δn_{film} ($=n_{\text{film}}-n_m$) was essentially constant irrespective of initial choice of d_{film} (or Δn_{film}). If this holds true also in the case of peak-position changes of LSPR-active NPs, any of the pairs of d and n capable of representing the peak-position change would be possible to use for a sufficiently good estimation of the mass uptake using Eq. (1). To test this hypothesis, the pairs of $d_{i,\text{film}}$ and $n_{i,\text{film}}$ that generated perfect representations of the peak-position changes were used to produce graphs in which $1/\Delta n_{i,\text{film}}$ is plotted versus $d_{i,\text{film}}$ within the following physically realistic thickness regimes: 1.5–3.5 nm for SH-COOH, 3–13 nm for PLL-g-PEG–PLL-g-PEGbiotin, and 3–7 nm for NeutrAvidin [Fig. 3(a)]. Note

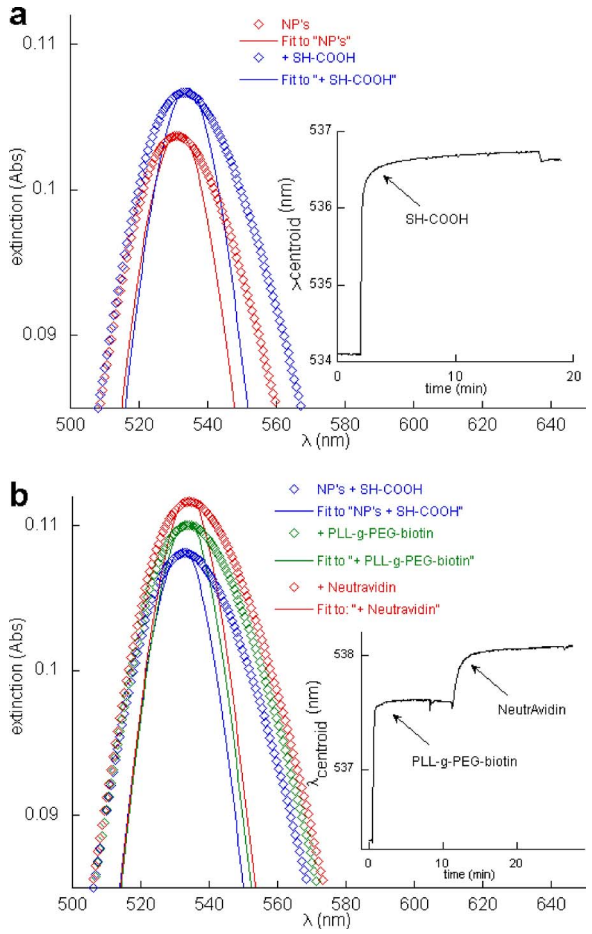

FIG. 2. UV-vis extinction spectra of Au NPs on glass upon formation of the three-layer surface architecture and theoretical representations of the data. (a) Experimental (open symbols) and theoretical (solid lines) extinction spectra for immobilized NPs immersed in ethanol before (red) and after (blue) saturated binding of SH-COOH. (b) Same type of data as in (a) but the SH-COOH-modified NPs immersed instead of in buffer before (blue) and after subsequent additions of (1:1) PLL-g-PEG–PLL-g-PEGbiotin (1.3 μM; green) and NeutrAvidin (0.8 μM; red). The fits were obtained using values of d and n of 2.2 nm and 1.49, 7 nm and 1.37, and 4.5 nm and 1.375 for layers 1, 2, and 3, respectively. The insets in (a) and (b) display the time evolution of changes in the peak position obtained via a centroid tracking algorithm (see main text), demonstrating that the $\Delta\lambda_{\text{centroid}}$ ($\propto\Delta\lambda_{\text{peak}}$) can, at a temporal resolution of better than 2 s, be recorded with a noise of less than $\sim 10^{-3}$ nm.

that in Eq. (1), $1/\Delta n_{i,\text{film}}$ scales linearly with $d_{i,\text{film}}$ with a proportionality constant equal to $\Gamma_i/(\partial n/\partial C)_i$.

It is seen in Fig. 3(a) that in the low-thickness regime of layer 1, the increment in $1/\Delta n$ scales linearly with the increment in d, while there is a clear deviation from linearity as the film thickness increases (see layers 2 and 3). This feature is attributed to the orders of magnitude more shallow penetration depth of the evanescent field of the plasmon polaritons associated with noble metal NPs, as previously observed experimentally[9,32,33,49] and described theoretically,[26] than that associated with laterally propagating SPR. As a consequence, in order to accurately determine the coupled mass using Eq. (1), it is of utmost importance that the thicknesses of the films are known or can be independently determined. This is illustrated in Fig. 3(b), displaying the mass uptake obtained using Eq. (1) for the pairs of $d_{i,\text{film}}$ and $n_{i,\text{film}}$ used to produce Fig. 3(a). Interestingly, in the case of SH-COOH, forming a densely packed film with a thickness of ~2.2 nm on planar Au,[37,48] the uncertainty in mass uptake is less than 4% in the chosen thickness regime (1.5–3 nm). Furthermore, using the film thickness of 2.2 nm, the absolute mass uptake becomes ~222 ng/cm^2, which is in perfect agreement with the expected value of ~224 ng/cm^2 for this type of SAM on a planar (111) gold surface [with an area coverage per SH-COOH molecule on gold (111) of 21.4 Å^2/chain (Ref. 33) and a molecular weight of 288.5 g/mol, the coupled mass of a SAM is ~224 ng/cm^2]. This extraordinary good agreement might be a lucky coincidence, since in reality, (i) the NPs are not perfectly spherical (see Fig. 1) but contain facets and grain boundaries likely to influence the local field strength and (ii) the amine-mediated immobilization of NPs to the substrate is, due to geometrical constrains, expected to reduce the available surface area by up to 10%. Since these two effects are expected to counteract each other in terms of induced peak-position change upon binding of organic material, the good agreement obtained makes it fair to state that the estimation in mass uptake is accurate to at least within ~10%.

For subsequent binding of PLL-g-PEG–PLL-g-PEGbiotin, the situation becomes more complicated. Although it is well established that the polylysine backbone of PLL-g-PEG mediates a firm binding to negatively charged surfaces such as oxides of transition metals,[34,35] the flexible nature of the PEG chains makes it hard to predict the film thickness. As a consequence, an uncertainty in the mass uptake of 60% is observed, ranging from 130 to 210 ng/cm^2 for a contracted (d_2=3 nm) to an extended (d_2=13 nm) state of the PEG chains, respectively [Fig. 3(b)]. In an attempt to independently estimate the film thickness, and thus reduce the uncertainty in the mass-uptake estimation, the binding of a 1:1 mixture of PLL-g-PEG and PLL-g-PEG-biotin on SH-COOH-modified planar gold was analyzed using QCM-D monitoring,[45,50] as summarized in Table I. (Also shown in Table I are results obtained using conventional SPR analysis of planar gold and the analysis of the LSPR data, as described in detail below.)

Using a Voigt-based analysis of the QCM-D data,[41] an effective acoustic thickness of ~7.0 nm was obtained for the PLL-g-PEG–PLL-g-PEGbiotin layer. Using this thickness as an input in the analysis of the LSPR data, a mass uptake [see Fig. 3(b)] of ~164 ng/cm^2 is obtained at saturated binding of this copolymer layer on SH-COOH-modified NPs. Interestingly, this value is also in excellent agreement with previous reported data[38] on Nb_2O_5 and SH-COOH-modified gold, for which values of 168 and 160 ng/cm^2 were obtained, as well as with in house SPR data on planar gold, for which a mass uptake of ~166 ng/cm^2 was obtained (Table I). These values all fall within the 10% uncertainty identified above, thus strengthening the validity of the theoretical approach employed to quantify peak-position changes in terms of mass uptake. Furthermore, the results clearly demonstrate the importance of being able to determine the film thickness, as

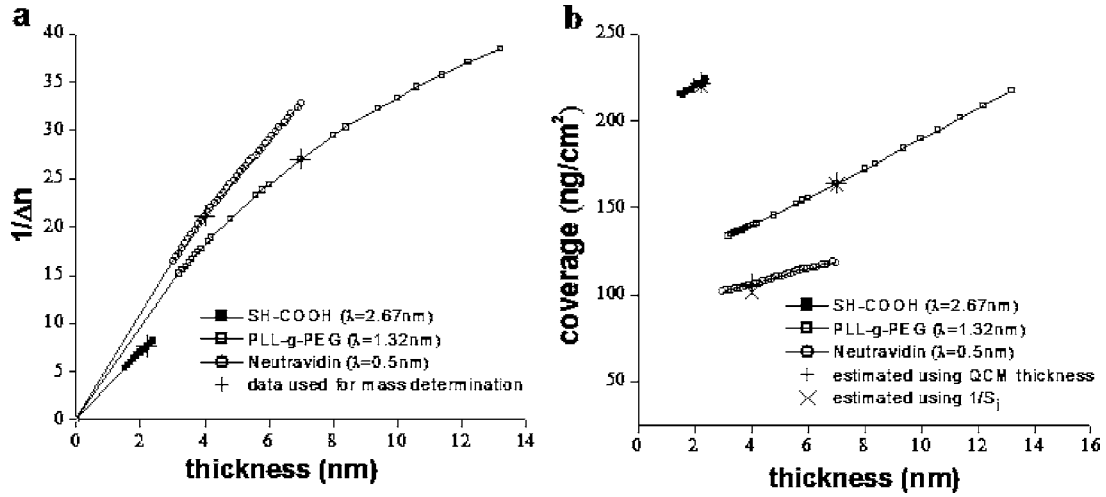

FIG. 3. Illustration of the relation between film refractive index, thickness, and mass obtained using the modeling shown in Fig. 2. (a) Film thickness d vs the inverse of the change in refractive index $[1/\Delta n = 1/(n_{\text{film}} - n_m)]$ for combinations of d and Δn which, using the core-shell model described in the main text, produce the observed peak-position changes, λ, for additions of (i) SH-COOH [Fig. 2(a)], (ii) PLL-g-PEGbiotin [Fig. 2(b)] and (iii) NeutrAvidin [Fig. 2(b)]. (b) Mass uptake estimated for the three layers using formalism De Feijter *et al.* [Eq. (1)] and the data shown in (a). The crosses represent the film thickness used to estimate the mass (see main text).

here done via QCM-D, in order to arrive at acceptable mass uptake estimations for LSPR-active NPs. (The much higher mass uptake obtained from QCM-D data measurements is due to water hydrodynamically[51] coupled to absorbed films, as discussed further below.)

Finally, by keeping the thicknesses (and refractive index) of layers 1 and 2 constant at 2.2 nm (1.49) and 7 nm (1.37), respectively, a mass uptake is obtained for NeutrAvidin that ranges from ~100 to ~120 ng/cm^2 for the lowest (3 nm) and highest (7 nm) possible thicknesses, respectively [Fig. 3(b)]. This, in turn, results in an uncertainty in the mass uptake of 20%. According to the QCM-D data, binding of NeutrAvidin results in an increase in effective thickness of 5.2 nm, thus proposing that the mass uptake is in this case ~108 ng/cm^2 [Fig. 3(b)]. This number is slightly lower than previous results (~120 ng/cm^2) obtained for NeutrAvidin binding on planar substrates modified with 1:1 mixtures of PLL-g-PEG and PLL-g-PEG-biotin.[38] It is, however, significantly lower than the mass uptake of 158 ng/cm^2 observed by us using SPR (Table I). One plausible explanation for this discrepancy is that NeutrAvidin does not form a homogeneous film on top of PLL-g-PEG–PLL-g-PEGbiotin, thus violating the core-shell model used in the theoretical representation. To test this hypothesis, PLL-g-PEG–PLL-g-PEGbiotin and NeutrAvidin were treated as one single layer, which increased in thickness from 7 to 12.2 nm (i.e., 7 +5.2 nm) upon NeutrAvidin binding. Using a total peak-position change of 1.82 nm (1.32+0.5 nm) and an effective

TABLE I. The responses for SPR, QCM-D and LSPR measurements.

	SPR		QCM-D			LSPR	
Layers	Response (RU)	Δm_{SPR}[a] (ng/cm^2)	Δf (Hz)	Δm[b] (ng/cm^2)	d[c] (nm)	$\Delta\lambda_{\text{centroid}}$[d] (nm)	Δm[e] (ng/cm^2)
SH-COOH	···	223.9[f]	···	···	···	2.67±0.53	221.8
PLL-g-PEG	2128±48	166±4[g]	−32.4±3.6	573±64	7	1.32±0.14	163.9
NeutrAvidin	2369±157	158±10	−31.1±2.2	550±39	5.2	0.50±0.07	108.2

[a]The SPR mass was estimated using the well-established relation between changes in resonance units (ΔRU) and mass uptake (1 RU=0.1 ng/cm^2) divided by 1.5 to take into account the fact that binding occurs on a planar surface, rather than an extended dextran hydrogel (Ref. 14).
[b]Obtained from a Voigt-based analysis of the QCM-D data.
[c]See footnote b.
[d]Absolute peak-position changes.
[e]Obtained from Fig. 3(b) with a thickness of SH-COOH of 2.2 nm (Ref. 48) and the thicknesses obtained from the QCM-D analysis of PLL-g-PEG and NeutrAvidin. The values of the refractive index increment were $(\partial n/\partial C)_{\text{COOH}}=0.1309$ cm^3/g (measured using an Abbe refractometer at 25 °C), $(\partial n/\partial C)_{\text{biotin-PLL-PEG}}=0.158$ cm^3/g (Ref. 36), and $(\partial n/\partial C)_{\text{NeutrAvidin}}=0.185$ cm^3/g (Ref. 56).
[f]Estimated using a surface coverage of 21.4 Å^2 per SH-COOH (Ref. 37).
[g]Estimated by correcting the mass-uptake conversion of SPR data for the differences in refractive index increment between PLL-g-PEG and proteins (Ref. 55).

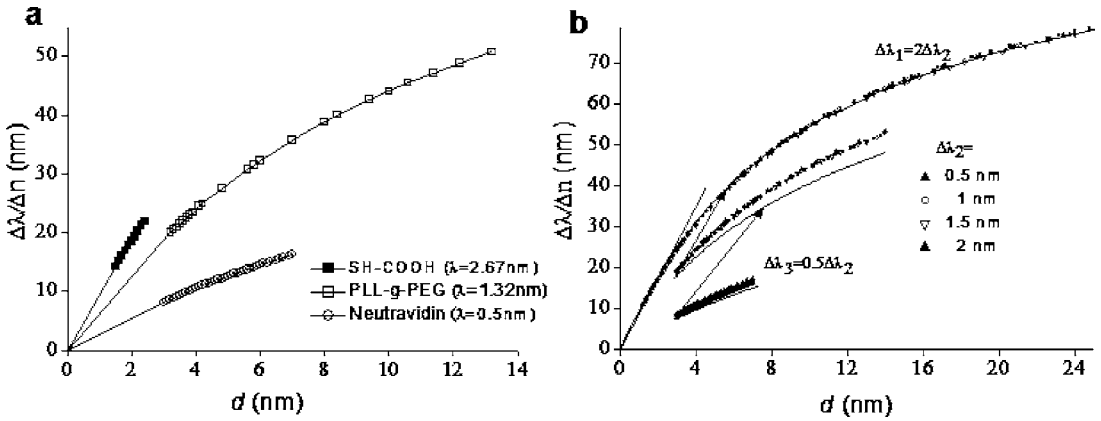

FIG. 4. Illustration of the generic applicability of the presented formalism for translation of peak-position changes into absolute mass uptake. (a) Same data as in Fig. 3(a) but represented by plotting film thickness versus $\Delta\lambda/\Delta n$. (b) Similar plot as (a) except that the arbitrary wavelength shifts for the first layer ($\Delta\lambda_1$,2,3,4 nm with corresponding varied layer thickness from 2.2 to 24 nm), for the second layer ($\Delta\lambda_2$=0.5,1,1.5,2 nm), and for the third layer ($\Delta\lambda_3$ =0.25,0.5,0.75,1 nm) were used to confirm that changes of $\Delta\lambda/\Delta n$ were independent of changes in $\Delta\lambda$ as well as Δn alone. The arrows indicate that the sensitivity functions $[S_i(d_i)]$ for layers 2 and 3 could be obtained by linear translations of $S_1(d_1)$ along the $\Delta\lambda/\Delta n$ and d axes using Eq. (7). To support a comparison with literature data and subsequent additions of biotinylated compounds (see main text), the sensitivity function for the first layer in (b) was obtained using water as the surrounding medium.

$\partial n/\partial C$ value of 0.1715 (corresponding to the mean of the $\partial n/\partial C$ values of PLL-g-PEG–PLL-g-PEGbiotin and NeutrAvidin), the increase in mass due to NeutrAvidin binding remains, however, at a value of $\sim$108 ng/cm^2 (not shown). Hence, regardless of whether the core-shell model is used or not, the mass uptake is lower than that observed on a planar surface. Hence, the lower mass uptake of NeutrAvidin on NPs is most likely a real effect, tentatively attributed to either the structure adopted by PLL-g-PEG–PLL-g-PEGbiotin on a surface with high curvature or to the difference in mass-transport conditions in the SPR and LSPR measurements. In the former case, a consequence of a surface with high (convex) curvature is that the PEG chains are expected to experience lower steric constrains than on a planar substrate, allowing the biotin moieties to become more available for interactions with any of the four biotin-specific sites on NeutrAvidin. This means, in turn, that early arriving NeutrAvidin molecules will have an increased tendency to be engaged in binding to multiple biotin moieties,[36] thus rapidly reducing the overall NeutrAvidin-binding capacity of the substrate. A similar result is also expected if the rate of arrival to the surface is low. Note, in particular, that in the case of NPs, the measurements were made from a stagnant solution, rendering mass-transport limited adsorption, while the SPR measurements were made in flow mode, utilizing microfluidics that have been previously shown to provide rapid and efficient transport properties.[17] The discrepancy in binding capacity between planar and nanoscale gold is thus considered real and not due to limitations of the theory used to represent the system.

B. Relation between peak-position change and mass uptake

In the analysis above, the mass uptake was estimated using pairs of d_i and Δn_i obtained via extensive numerical fitting procedures. Preferably, an analytical, or at least semi-analytical, expression capable of providing a direct relation between peak-position changes, $\Delta\lambda$, and coupled mass is desired. To meet this demand, we introduce in this section a generic expression capable of translating changes in peak position into mass uptake. Note first that if the relation obtained between $1/\Delta n_{\text{film}}$ and d_{film} [see Fig. 3(a)] is extended to include also the experimentally observed peak-position changes, $\Delta\lambda$, Eq. (1) can be rewritten as

$$\Gamma = \frac{d_i \Delta\lambda_i}{S_i(d_i)\partial n/\partial C}, \tag{2}$$

where $S_i(d_i)=\Delta\lambda_i/\Delta n_i$ is defined as the sensitivity function as shown in Fig. 4(a).

Furthermore, $S_i(d_i)$ (for i=1, 2, and 3) illustrated in Fig. 4(a) were obtained through a numerical fitting procedure based on the experimentally observed peak-position changes of 2.67, 1.32, and 0.5 nm for layers 1, 2, and 3, respectively. Hence, it is not fully clear whether Eq. (2) is applicable to arbitrary adsorption events. For example, what happens when the accompanied peak-position changes differ substantially from the ones used to generate Fig. 4(a)? To evaluate the general applicability of the obtained sensitivity curves, identical fitting procedures as those used to generate the data in Fig. 4(a) were made for arbitrary peak-position shifts, ranging from 0.25 to 4 nm for all three layers [Fig. 4(b)]. Strikingly, the sensitivity functions are, to a very good accuracy, independent of the experimentally observed peak-position shifts. This means, in turn, that Eq. (2) can be used to estimate the mass uptake irrespective of the magnitude of experimentally observed peak-position changes, with the important implication that Eq. (2) can be generically used to estimate temporal variations in coverage, i.e., $\Gamma(\lambda_i(t))$.

Still, for others to fully appreciate and make efficient use of these findings, it is important also to derive a mathematical description of $S_i(d_i)$. A *single-layered* sphere was therefore interpreted in the Rayleigh limit ($r_0 \ll \lambda$), in which case

the dipole resonance condition can be approximated as $\mathrm{Re}(\varepsilon_{\mathrm{Au}})+2n_{\mathrm{eff}}^2=0$, where $\mathrm{Re}(\varepsilon_{\mathrm{Au}})\approx a-b\lambda$ within the wavelength range of interest. Accordingly, the peak-position shift, $\Delta\lambda$, induced by a thin adsorbed film can, to a first approximation, be expressed as

$$\Delta\lambda = 2/b(n_{\mathrm{eff}}^2 - n_m^2). \tag{3}$$

Furthermore, in the Rayleigh limit, the local optical intensity decays approximately as $I_{\mathrm{loc}}\sim(r_0/r)^6$, where r is the distance from the center of the metal particle. A change in interfacial refractive index n_{film} induced by a single film with a thickness d_{film} can then be approximated as a change in the effective refractive index of the surrounding medium, n_{eff}, using a weighted average of the film and the medium:

$$\begin{aligned} n_{\mathrm{eff}} &= \frac{n_1\int_{r_0}^{r_0+d} 4\pi r^2(r_0/r)^6 dr + n_m\int_{r_0+d}^{\infty} 4\pi r^2(r_0/r)^6 dr}{\int_{r_0}^{\infty} 4\pi r^2(r_0/r)^6 dr} \\ &= n_1 - \frac{n_1-n_m}{(1+d/r_0)^3} = n_m + \left(1-\frac{1}{(1+d/r_0)^3}\right)\Delta n. \end{aligned} \tag{4}$$

Inserting Eq. (4) in Eq. (3) then gives

$$\begin{aligned} \Delta\lambda &\approx \frac{4n_m}{b}\left(1-\frac{1}{(1+d/r_0)^3}\right)\Delta n \\ &\quad + O\left(\frac{2}{b}\left(1-\frac{1}{(1+d/r_0)^3}\right)^2\Delta n^2\right) \\ &\approx \frac{4n_m}{b}\left(1-\frac{1}{(1+d/r_0)^3}\right)\Delta n, \end{aligned} \tag{5}$$

and thus

$$\begin{aligned} S(d) = \frac{\Delta\lambda}{\Delta n} &\approx \frac{4n_m}{b}\left(1-\frac{1}{(1+d/r_0)^3}\right)^{\text{Taylor expansion}} \\ &\approx c_1 d + c_2 d^2 + c_3 d^3 + c_4 d^4 + c_5 d^5 + O(d^n), \end{aligned} \tag{6}$$

where $c_1=12n_m/br_0$ and $c_i\propto 1/r_0^i$. To achieve representative values of c_i, a least square fit between Eq. (6) and $S_1(d)$ in Fig. 4(b) was made, yielding values of c_1, c_2, c_3, c_4, and c_5 of 10.25, -0.757, 36.2×10^{-3}, -0.95×10^{-3}, and 10.3×10^{-6}, respectively. Interestingly, with $b=0.07$ nm^{-1} (the value was adopted by Johnson and Christy[52]), $r_0=20$ nm, and $n_m=1.333$, c_1 becomes 11.4. This is fairly close to the value of 10.25 obtained from the fit to the curve generated through the more accurate theoretical analysis, thus supporting the physical validity of the simplified mathematical representation. Also note that $S(d)$ *cannot* be perfectly represented by a single exponential function, as previously used to approximate the field-intensity decay versus distance from the metal-solution interface.[33]

A further inspection of the $S_i(d_i)$ curves for the three layers also reveals that $S_{i>1}$ can, to a good approximation, be obtained by linear translations of $S_1(d)$ along the $\Delta\lambda/\Delta n$ and d axes, respectively [solid lines in Fig. 4(b)]. This means, in turn, that the sensitivity functions for the outer layers can be obtained directly from $S(d)$:

$$S_i(d_i) = S\left(d_i + \sum_{j=1}^{i-1} d_j\right) - S\left(\sum_{j=1}^{i-1} d_j\right), \tag{7}$$

where $S(d)$ is given by Eq. (6). Hence, $S_i(d_i)$ does not depend strongly on either experimentally observed peak-position shifts or refractive index values of the layers used in the core-shell model. This thus proves the general applicability of absolute mass-uptake estimations using the proposed formalism, as illustrated in the following section by comparing the temporal variation in mass uptake with that obtained using SPR and QCM-D upon immunocomplex formation utilizing a biotinylated scFv antibody. Note, too, that the sensitivity functions derived in this work are applicable for gold NPs with a mean diameter of 40 nm, but the dependence of the explicit dependence on particle radius [Eq. (6)] allows the formalism to be extended to arbitrary NP with diameters $<\sim 50$ nm.

C. Quantification of the temporal variations in peak-position changes in terms of mass uptake

The sensitivity function arrived at above was used to analyze the temporal variation in mass uptake. It is first worthwhile to note, though, that this sensitivity function is consistent with previous studies in which, for example, multilayer formation was used to probe the sensing depth of similar LSPR-active substrates. Note, in particular, the almost perfect agreement with the results obtained by Nath and Chilkoti[9] for polyelectrolyte multilayers on NPs with a diameter essentially identical to that used by us. In their study, they also investigated streptavidin binding to a biotinylated SAM similar to the SH-COOH SAM used in our study. Translating the increment in extinction magnitude at $\lambda\sim575$ nm observed by them into peak-position changes, the use of Eqs. (2), (6), and (7) gives a mass uptake of streptavidin of 210 ng/cm^2. This is indeed in perfect agreement with previous data on streptavidin binding on biotin-modified SAMs on gold,[53] further supporting the validity of the theoretical representations presented in this work. Furthermore, since the sensitivity function was proven to be independent of the magnitude of peak-position changes (see above), Eqs. (2), (6), and (7) can, to a very good approximation, be used for a direct conversion of $\Delta\lambda_{\mathrm{centroid}}(t)$ into mass uptake, $\Gamma(t)$. This is illustrated in Fig. 5, displaying $\Gamma(t)$ upon exposure of SH-COOH-modified NPs to PLL-g-PEG–PLL-g-PEGbiotin and NeutrAvidin, under the assumptions that the layers of SH-COOH, PLL-g-PEG–PLL-g-PEGbiotin, and NeutrAvidin have thicknesses of 2.2, 7, and 4.5 nm, respectively (see above). Also shown in Fig. 5 is the mass uptake versus time obtained using QCM-D and conventional SPR measurements.

Besides illustrating the possibility of using LSPR-active templates to quantify, for example, binding kinetics as well as stoichiometric relations for interacting entities of different

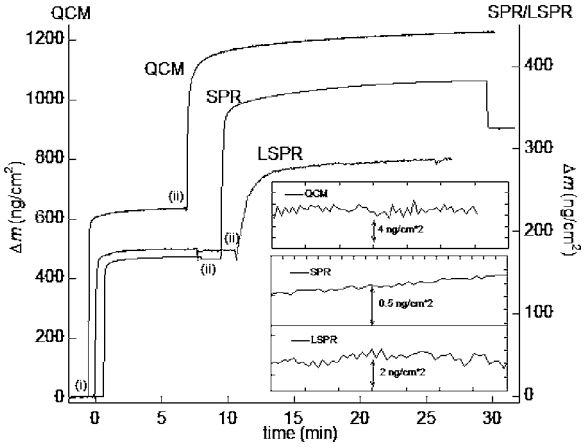

FIG. 5. Mass uptake, Δm, vs time for LSPR, SPR, and QCM upon addition of (i) PLL-g-PEG–PLL-g-PEGbiotin (1:1) and (ii) NeutrAvidin, a buffer rinsing step was performed before and after injection of sample solutions (i) and (ii), respectively. The coupled mass was estimated as in Table I for SPR and QCM, while the LSPR data were estimated using Eqs. (2), (6), and (7), with d_i values of 2.2, 7, 5.2 nm for SH-COOH, PLL-g-PEG, and NeutrAvidin, respectively. The insets display the signal-to-noise levels for the respective three techniques.

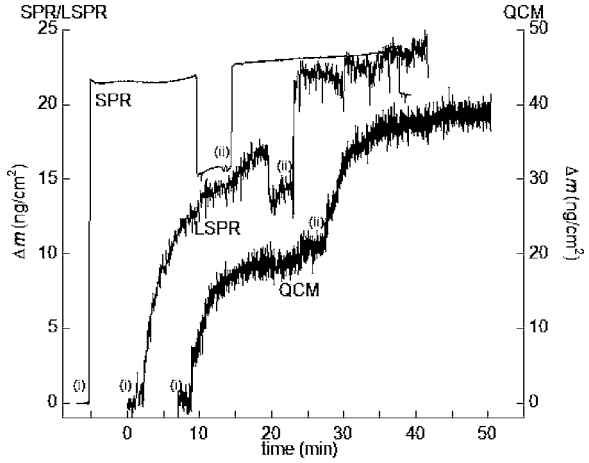

FIG. 6. Same type of data as in Fig. 5 but for subsequent additions of (i) scFv and (ii) cholera toxin to the sensor template. The coupled mass was estimated as in Table I for SPR and QCM, while the LSPR data were estimated using Eqs. (2), (6), and (7), with d_i values of 2.2, 7, 5.2, 2, and 5 nm for SH-COOH, PLL-g-PEG, NeutrAvidin, scFv, and cholera toxin, respectively.

types, these data also provide a basis for a comparison between the sensitivities of the different sensor systems used in this study. For the LSPR sensor, the noise level is approximately 2 ng/cm^2, which is approximately a factor of 8 higher than that of the commercial SPR system (BIAcore 2000), but a factor of 2 lower than that of the commercial QCM-D system (Q-Sense D300) (see insets in Fig. 5). However, to estimate signal-to-noise ratios, one must also take into account the obtained signals. While the saturated signals (after rinsing) are fairly similar for SPR and LSPR, the mass uptake obtained using QCM-D is almost a factor of 4 larger than that obtained using SPR and LSPR. This means, in turn, that the signal-to-noise ratio is a factor of $\sim$2 better for QCM-D than for LSPR. Note, however, that in contrast to the SPR data, neither LSPR nor QCM-D suffers from significant steps upon exchange between protein solutions and buffer solutions. This is most clearly seen in Fig. 5 upon rinsing in buffer after saturated binding of NeutrAvidin and is attributed to the fact that (i) due to the significantly larger penetration depth of the evanescent field of SPR compared with LSPR, SPR is more sensitive to changes in bulk-refractive index induced by dissolved molecules and (ii) SPR is more sensitive to changes in bulk-refractive index than QCM-D is to corresponding changes in bulk viscosity/density. Hence, to probe binding kinetics, it is in the cases of LSPR and QCM much less critical to operate with reference channels capable of compensating for changes in the bulk properties due to, for example, dissolved molecules. Furthermore, the LSPR data were obtained with a measurement cell that was not temperature stabilized, while both the SPR and the QCM-D measurements require measurement chambers with a temperature control of better than 1×10^{-2} °C. Hence, the (i) high precision by which peak-position changes ($<5\times10^{-3}$ nm) can be recorded using a low cost ($<\$5000$) spectrophotometer setup, (ii) good agreement between the absolute mass uptake between LSPR and SPR, and (iii) low sensitivity to variations in bulk-refractive index, induced by, for example, dissolved molecules or temperature fluctuations make the LSPR sensing concept highly attractive as an alternative to the more well-established commercially available concepts. Especially with the consideration of the capability of using individual NPs to probe zeptomol quantities of bound molecules,[5,6] it further points towards the development of extremely miniaturized sensors. Note, however, that substantial efforts must still be made before similar noise levels in terms of adsorbed mass per unit area are reached for individual NPs.

A potential drawback with the LSPR sensors is, however, the rapidly diminishing sensitivity versus distance from the metal-solution interface, putting strong constrains on the molecular dimensions of the probed entities. For instance, although thin ($\sim$2 nm) SAMs of thiolated PEGs have been shown to be relatively inert with respect to unspecific protein adsorption,[54] the thicker ($\sim$7 nm) films of PLL-g-PEG provide superior protein resistant properties.[34,35] As low unspecific protein adsorption is a key requirement in any sensor application, PLL-g-PEG is a preferable choice. However, if NeutrAvidin is used as a linker for subsequent coupling of biotinylated compounds, the latter will, by necessity, bind in a region where the sensitivity is significantly reduced. Hence, to probe, for example, immunoreactions, this means that the molecules engaged in the biorecognition reaction must be carefully matched to the sensitivity function. For instance, to probe immunoreactions, relatively bulky ($\sim$10 nm) IgG antibodies are generally utilized. Since this would force the immunocomplex to be formed at a distance outside the evanescent field of the NPs, we utilized instead a single-chain antibody fragment, scFv (CT17, MW $\sim$28 kDa, $\varnothing\sim$2 nm) directed against cholera toxin, CT. Addition of CT17 followed by rinsing and addition of CT is shown in Fig. 6, together with the mass uptake

versus time obtained using SPR and QCM-D for the same sequence of events.

Due to the overall low mass uptake in these steps compared with the previously formed layers, the steplike behavior upon solution exchange (for example, from protein solution to buffer solution) observed in the SPR data complicates an analysis of binding kinetics. In contrast, both LSPR and QCM-D display less significant steps upon solution exchange, and due to the slower binding obtained in batch rather than flow mode enables binding kinetics to be evaluated. Note also that a good agreement in saturated mass uptake was obtained from LSPR and SPR, whereas the QCM-D yields a higher mass uptake also in this case. In addition the mass uptake of scFv (CT17) is approximately a factor of 2 lower than expected for one-to-one binding ratio between CT17 (28 kDa) and NeutrAvidin (65 kDa). This is consistent with previous results on coupling of biotinylated IgG to PLL-g-PEG–PLL-g-PEGbiotin-modified surfaces[36] and is attributed to cross-linking, i.e., the ability of the biotin moieties on the flexible PEG chains to efficiently occupy the four biotin-binding sites of NeutrAvidin.[36] Still, the results show that with a proper choice of recognition elements, the LSPR sensing concept is compatible with immunosensing utilizing a sensor template with undetectable nonspecific binding from complex suspensions such as serum. In forthcoming studies this will be utilized in sensor designs exploring the compatibility of LSPR with high miniaturization (see Ref. 57).

ACKNOWLEDGMENTS

Financial support was obtained from the Biomimetic Material Science program and The Ingvar grant, both funded by the Swedish Foundation for Strategic Research.

[1]N. Ramachandran, D. N. Larson, P. R. H. Stark, E. Hainsworth, and J. LaBaer, FEBS J. **272**, 5412 (2005).
[2]E. Hutter and J. H. Fendler, Adv. Mater. (Weinheim, Ger.) **16**, 1685 (2004).
[3]A. J. Haes and R. P. Van Duyne, Anal. Bioanal. Chem. **379**, 920 (2004).
[4]P. Englebienne, Analyst (Cambridge, U.K.) **123**, 1599 (1998).
[5]G. Raschke, S. Kowarik, T. Franzl, C. Sonnichsen, T. A. Klar, J. Feldmann, A. Nichtl, and K. Kurzinger, Nano Lett. **3**, 935 (2003).
[6]A. D. McFarland and R. P. Van Duyne, Nano Lett. **3**, 1057 (2003).
[7]N. N. Kariuki *et al.*, Langmuir **20**, 11240 (2004).
[8]H. E. Ruda and A. Shik, Phys. Rev. B **71**, 245328 (2005).
[9]N. Nath and A. Chilkoti, Anal. Chem. **76**, 5370 (2004).
[10]K. L. Kelly, E. Coronado, L. L. Zhao, and G. C. Schatz, J. Phys. Chem. B **107**, 668 (2003).
[11]I. O. Sosa, C. Noguez, and R. G. Barrera, J. Phys. Chem. B **107**, 6269 (2003).
[12]W. Rechberger, H. A. Leitner, J. R. Krenn, B. Lamprecht, and F. R. Aussenegg, Opt. Commun. **220**, 137 (2003).
[13]A. J. Haes, S. Zou, G. C. Schatz, and R. P. Van Duyne, J. Phys. Chem. B **108**, 6961 (2004).
[14]B. Liedberg, I. Lundström, and E. Stenberg, Sens. Actuators B **11**, 63 (1993).
[15]W. Hickel and M. Knoll, J. Appl. Phys. **67**, 3572 (1990).
[16]B. P. Nelson, A. G. Frutos, J. M. Brockman, and R. M. Corn, Anal. Chem. **71**, 3928 (1999).
[17]E. Stenberg, B. Persson, H. Ross, and C. Urbaniczky, J. Colloid Interface Sci. **143**, 513 (1991).
[18]L. S. Jung, C. T. Campbell, T. M. Chinowsky, M. N. Mar, and S. S. Yee, Langmuir **14**, 5636 (1998).
[19]G. Kalyuzhny, M. A. Schneeweiss, A. Shanzer, A. Vaskevich, and I. Rubinstein, J. Am. Chem. Soc. **123**, 3177 (2001).
[20]G. Kalyuzhny, A. Vaskevich, M. A. Schneeweiss, and I. Rubinstein, Chem.-Eur. J. **8**, 3850 (2002).
[21]M. D. Malinsky, K. L. Kelly, G. C. Schatz, and R. P. Van Duyne, J. Am. Chem. Soc. **123**, 1471 (2001).
[22]A. J. Haes and R. P. Van Duyne, J. Am. Chem. Soc. **124**, 10596 (2002).
[23]J. C. Riboh, A. J. Haes, A. D. McFarland, C. R. Yonzon, and R. P. Van Duyne, J. Phys. Chem. B **107**, 1772 (2003).
[24]H. Kitano, Y. Anraku, and H. Shinohara, Biomacromolecules **7**, 1065 (2006).
[25]E. Reimhult, C. Larsson, B. Kasemo, and F. Hook, Anal. Chem. **76**, 7211 (2004).
[26]H. X. Xu and M. Käll, Sens. Actuators B **87**, 244 (2002).
[27]L. Olofsson, T. Rindzevicius, I. Pfeiffer, M. Käll, and F. Höök, Langmuir **19**, 10414 (2003).
[28]T. R. Jensen, G. C. Schatz, and R. P. Van Duyne, J. Phys. Chem. B **103**, 2394 (1999).
[29]T. R. Jensen, M. L. Duval, K. L. Kelly, A. A. Lazarides, G. C. Schatz, and R. P. Van Duyne, J. Phys. Chem. B **103**, 9846 (1999).
[30]J. A. De Feijter, J. Benjamins, and F. A. Veer, Biopolymers **17**, 1759 (1978).
[31]C. R. Yonzon, E. Jeoung, S. Zou, G. C. Schatz, M. Mrksich, and R. P. Van Duyne, J. Am. Chem. Soc. **126**, 12669 (2004).
[32]I. Doron-Mor, H. Cohen, Z. Barkay, A. Shanzer, A. Vaskevich, and I. Rubinstein, Chem.-Eur. J. **11**, 5555 (2005).
[33]A. J. Haes, S. Zou, G. C. Schatz, and R. P. Van Duyne, J. Phys. Chem. B **108**, 109 (2004).
[34]S. Pasche, S. M. De Paul, J. Vörös, N. D. Spencer, and M. Textor, Langmuir **19**, 9216 (2003).
[35]G. L. Kenausis *et al.*, J. Phys. Chem. B **104**, 3298 (2000).
[36]N. P. Hung, J. Vörös, S. M. De Paul, M. Textor, and N. D. Spencer, Langmuir **18**, 220 (2002).
[37]L. Strong and G. M. Whitesides, Langmuir **4**, 546 (1988).
[38]F. Xu, G. Zhen, M. Textor, and W. Knoll, BioInterphases **1**, 73 (2006).
[39]K. Johansen, I. Lundström, and B. Liedberg, Biosens. Bioelectron. **15**, 503 (2000).
[40]A. Dahlin, M. Zach, T. Rindzevicius, M. Kall, D. S. Sutherland, and F. Hook, J. Am. Chem. Soc. **127**, 5043 (2005).
[41]F. Höök, B. Kasemo, T. Nylander, C. Fant, K. Sott, and H. Elwing, Anal. Chem. **73**, 5796 (2001).
[42]A. Zdanov, Y. Li, D. R. Bundle, S. J. Deng, R. Mackenzie, S. A. Narang, N. M. Young, and M. Cygler, Proc. Natl. Acad. Sci. U.S.A. **91**, 6423 (1994).
[43]E. Söderlind *et al.*, Nat. Biotechnol. **18**, 852 (2000).
[44]C. Wingren, C. Steinhauer, J. Ingvarsson, E. Persson, K. Larsson, and C. A. K. Borrebaeck, Proteomics **5**, 1281 (2005).
[45]F. Höök, M. Rodahl, P. Brzezinski, and B. Kasemo, Langmuir **14**, 729 (1998).
[46]H. X. Xu, Phys. Rev. B **72**, 073405 (2005).
[47]A. Dahlin, J. O. Tegenfeldt, and F. Höök, Anal. Chem. **78**, 4416 (2006).
[48]C. D. Bain, E. B. Troughton, Y. T. Tao, J. Evall, G. M. Whitesides, and R. G. Nuzzo, J. Am. Chem. Soc. **111**, 321 (1989).
[49]D. D. Evanoff, Jr. and G. Chumanov, ChemPhysChem **6**, 1221 (2005).
[50]M. Rodahl, F. Höök, and B. Kasemo, Anal. Chem. **68**, 2219 (1996).
[51]F. Höök *et al.*, Colloids Surf., B **24**, 155 (2002).
[52]P. B. Johnson and R. W. Christy, Phys. Rev. B **6**, 4370 (1972).
[53]G. Stengel and W. Knoll, Nucleic Acids Res. **33**, e69 (2005).
[54]S. J. Sofia, V. Premnath, and E. W. Merrill, Macromolecules **31**, 5059 (1998).
[55]T. M. Davis and W. D. Wilson, Anal. Biochem. **284**, 348 (2000).
[56]J. Vörös, J. J. Ramsden, G. Csúcs, I. Szendro, S. M. De Paul, M. Textor, and N. D. Spencer, Biomaterials **23**, 3699 (2002).
[57]See EPAPS Document No. E-BJIOBN-2-002701 for a description of the slightly modified extended Mie theory. This document can be reached via a direct link in the online article's HTML reference section or via the EPAPS homepage (http://www.aip.org/pubservs/epaps.html).